Published in final edited form as:
Nature. 2010 November 25; 468(7323): 527–532. doi:10.1038/nature09606.

Sugar transporters for intercellular exchange and nutrition of pathogens

Li-Qing Chen[1], **Bi-Huei Hou**[1], **Sylvie Lalonde**[1], **Hitomi Takanaga**[1], **Mara L. Hartung**[1], **Xiao-Qing Qu**[1], **Woei-Jiun Guo**[1], **Jung-Gun Kim**[2], **William Underwood**[4], **Bhavna Chaudhuri**[1], **Diane Chermak**[1], **Ginny Antony**[3], **Frank F. White**[3], **Shauna C. Somerville**[4], **Mary Beth Mudgett**[2], and **Wolf B. Frommer**[1]

[1] Department of Plant Biology, Carnegie Institution for Science, 260 Panama St, Stanford, California 94305, USA

[2] Department of Biology, Stanford University, 228A Gilbert Bioscience Building, 371 Serra Mall, Stanford, California 94305, USA

[3] Department of Plant Pathology, Kansas State University, Manhattan, Kansas 66506, USA

[4] Energy Bioscience Institute, 130 Calvin Hall, MC 5230, Berkeley, California 94720, USA

Abstract

Sugar efflux transporters are essential for the maintenance of animal blood glucose levels, plant nectar production, and plant seed and pollen development. Despite broad biological importance, the identity of sugar efflux transporters has remained elusive. Using optical glucose sensors, we identified a new class of sugar transporters, named SWEETs, and show that at least six out of seventeen *Arabidopsis*, two out of over twenty rice and two out of seven homologues in *Caenorhabditis elegans*, and the single copy human protein, mediate glucose transport. *Arabidopsis* SWEET8 is essential for pollen viability, and the rice homologues SWEET11 and SWEET14 are specifically exploited by bacterial pathogens for virulence by means of direct binding of a bacterial effector to the SWEET promoter. Bacterial symbionts and fungal and bacterial pathogens induce the expression of different *SWEET* genes, indicating that the sugar efflux function of SWEET transporters is probably targeted by pathogens and symbionts for nutritional gain. The metazoan homologues may be involved in sugar efflux from intestinal, liver, epididymis and mammary cells.

The molecular nature of cellular sugar efflux in both plants and animals is unknown despite the fact that sugar efflux is an essential component for cellular exchange of carbon and energy in multicellular organisms[1–4]. Sugar efflux from the tapetum or transmitting tract of the style, for example, fuels pollen development and pollen tube growth[5]. Flowers secrete sugars for nectar production to attract pollinators, and plants secrete carbohydrates into the rhizosphere, potentially to feed beneficial microorganisms[6]. Sugar efflux carriers are

Correspondence and requests for materials should be addressed to W.B.F. (wfrommer@carnegiescience.edu).

Full Methods and any associated references are available in the online version of the paper at www.nature.com/nature.

Supplementary Information is linked to the online version of the paper at www.nature.com/nature.

Author Contributions W.B.F., S.L., M.B.M. and S.C.S. conceived and designed the experiments. L.-Q.C., B.-H.H., H.T., M.L.H., J.-G.K., X.-Q.Q., W.-J.G., W.U., B.C., G.A. and D.C. performed the experiments. W.B.F., S.L., M.B.M., G.A., F.F.W. and S.S. analysed the data. L.-Q.C. and W.B.F. wrote the manuscript.

Author Information Reprints and permissions information is available at www.nature.com/reprints. The authors declare no competing financial interests. Readers are welcome to comment on the online version of this article at www.nature.com/nature.

required at other sites, including mesophyll in leaves and the seed coat[7]. In mammals, glucose efflux from liver is crucial for the maintenance of blood glucose levels[2].

The primary goal of pathogens is to access nutrients from their hosts for reproduction. Phytopathogenic bacteria in the genera *Pseudomonas* and *Xanthomonas* can live in the intercellular space (apoplasm) of plants, where they acquire carbohydrates for energy and carbon[8]. Successful pathogens probably co-opt nutrient efflux mechanisms of the host to redirect nutrient flux[9]. Plants and pathogens engage in an evolutionary tug-of-war, in which the plant limits pathogen access to nutrients and initiates immune responses, whereas the pathogen evolves adaptive strategies to gain access to nutrients and suppress host immunity. Insight into mechanisms used by pathogens to alter plant immunity is emerging. However, the mechanisms that pathogens use to alter host physiology, notably efflux of sugars to support growth, are poorly understood. We hypothesize that sugar efflux transporters are co-opted by pathogens to supply nutrients[9]. This hypothesis is supported by studies of sugar transfer from wheat leaves to powdery mildew[10–12]. Pathogen glucose/H^+ uptake transporters have been identified[13]; by contrast, plant sugar efflux mechanisms have remained elusive.

Identification of AtSWEET1 as a glucose uniporter

To identify new transporters potentially involved in glucose efflux, we screened genes encoding uncharacterized polytopic membrane proteins from the *Arabidopsis* membrane protein database Aramemnon[14] using a new mammalian expression system[15]. Candidate genes were co-expressed with the high-sensitivity fluorescence resonance energy transfer (FRET) glucose sensor, FLIPglu600μΔ13V, in human HEK293T cells, which have low endogenous glucose uptake activity[15,16]. Among the genes tested, *AtSWEET1* (AT1G21460) expression enabled HEK293T cells to accumulate glucose as detected by a glucose-induced negative FRET ratio change (Fig. 1a). To determine whether AtSWEET1 also mediates efflux from the cytosol, the FRET glucose sensor FLIPglu600μΔ13V^{ER} was expressed in the lumen of the endoplasmic reticulum (ER; Fig. 1b). Topologically, efflux across the plasma membrane from the cytoplasmic side is equivalent to efflux into the ER that is also initiated from the cytoplasmic side (Fig. 1c). The glucose-dependent response of the ER sensor demonstrates that AtSWEET1 can mediate both uptake across the plasma membrane and efflux into the ER. SWEET1 thus seems to function as a bidirectional uniporter/facilitator. The observed sugar uptake and efflux were not due to subcellular re-localization of the FRET sensors (Supplementary Fig. 1). A carboxy-terminal green fluorescent protein (GFP) fusion of AtSWEET1 was functional in cellular uptake and localized to the plasma membrane of HEK293T cells (Supplementary Fig. 2). AtSWEET1 carrying a premature stop codon at position 198 was non-functional (Supplementary Fig. 3). Induction of endogenous GLUT glucose transporters in AtSWEET1-expressing HEK293T cells was excluded based on insensitivity of uptake to the GLUT inhibitor cytochalasin B (Supplementary Fig. 4a, b) and lack of detectable changes of messenger RNA levels of known human GLUT and SGLT glucose transporters (Supplementary Fig. 4c). The transport function of AtSWEET1 was independently demonstrated by expression in a yeast mutant lacking all 18 hexose transporters[17]. AtSWEET1 enabled the yeast mutant to grow on glucose (Fig. 1d) and to accumulate intracellular glucose as determined with the FRET glucose sensor FLII^{12}Pglu700μδ6 (ref. [18]) (Fig. 1e). AtSWEET1 functions as a low-affinity glucose transporter (Michaelis constant (K_m) ~9 mM; Fig. 1f). Consistent with a uniport transport mechanism, uptake was largely pH-independent (Supplementary Fig. 5). AtSWEET1 did not efficiently complement mannose, fructose and galactose uptake deficiencies of the mutant (Supplementary Fig. 6). Radiotracer experiments in *Xenopus* oocytes were used as another measure for AtSWEET1 sugar uptake activity (Fig. 1g). Direct proof for efflux activity was obtained by monitoring time-dependent release of [^{14}C]glucose from oocytes after injection

of radiotracer (Fig. 1h). In support of the function in cellular uptake and efflux, a constitutively expressed AtSWEET1–yellow fluorescent protein (YFP) fusion localized to the plasma membrane in *Arabidopsis* leaves (Fig. 1i). On the basis of expression studies, *AtSWEET1* is highly expressed in *Arabidopsis* flowers, where the protein may supply nutrients to the gametophyte or nectaries (Supplementary Fig. 7). The biochemical properties of AtSWEET1 are markedly similar to an unidentified transport activity characterized in roots using FRET sensors[19]. However, At*SWEET1* expression in roots was low, implicating other AtSWEET paralogues for this function.

SWEET1 belongs to a novel transporter family (PFAM PF03083) with 17 members in *Arabidopsis* and ~21 in rice (Supplementary Fig. 8). SWEETs fall into four subclades (Supplementary Fig. 8a) with 27–80% identity (Supplementary Fig. 8b). SWEETs are small proteins predicted to form a pore from seven transmembrane helices (Supplementary Fig. 9). Modelling indicates that the structure results from an ancient duplication of a 3-transmembrane-helix-domain polypeptide (1–3 and 5–7) fused via transmembrane helix 4 in a 3+ 1+3 configuration (Fig. 1j).

Diverse roles for SWEET paralogues

The phenotypes of several *sweet* mutants have been described. AtSWEET1 (clade 1) is 42% identical to its paralogue AtSWEET8 (clade 2) (Supplementary Fig. 8b). *AtSWEET8* (also called *RPG1*) is expressed in the tapetum[20], and mutation of *AtSWEET8* causes male sterility, compatible with a role in glucose efflux for pollen nutrition[20].

AtSWEET1 and AtSWEET8 share 31% and 34% amino acid sequence identity with rice OsSWEET11 (also called Os8N3 or Xa13; here named OsSWEET11 based on phylogeny)[21]. Similar to AtSWEET8, OsSWEET11 contributes to pollen viability, as RNA interference to OsSWEET11 reduced starch content in pollen and caused male sterility in rice[21] (Supplementary Fig. 8b). Expression studies indicate that the import function of SWEETs may also contribute to the nutrition of growing pollen tubes. Specifically, *AtSWEET1* is expressed in hydrated pollen and both *AtSWEET1* and *AtSWEET8* are expressed highly in pollen tubes[22]. *AtSWEET5* (also called *VEX1*) is expressed in mature, hydrated and germinating pollen and is found specifically in the vegetative cell of pollen grains, which may supply the generative cell with sugars[23]. Silencing of the clade 3 SWEET homologue *NEC1* from petunia also triggered male sterility[24]. *NEC1* is expressed in nectaries, and developmental regulation of *NEC1* correlates inversely with nectarial starch content, indicating a second function for NEC1 in sugar secretion in nectaries[25]. Hexoses, in particular galactose, fructose and glucose, accumulate in senescent leaves, and SWEET members may also function in mobilization of carbohydrate during senescence[26]. The *AtSWEET15* (also called *SAG29*) gene is induced ~22-fold in leaves during senescence[27]. Taken together, the SWEET sugar transporters probably supply carbohydrates to a variety of tissues in both monocotyledonous and dicotyledonous plants. Other SWEET members also function in glucose transport. For example, co-expression of AtSWEET8 with FRET sensors FLIPglu600μΔ13V or FLIPglu600μΔ13V^{ER} in HEK293T cells leads to glucose transport across both plasma and ER membranes (Supplementary Fig. 10), and AtSWEET8 complements the yeast glucose transport mutant (Fig. 1d and Supplementary Figs 5 and 11). At least four additional *Arabidopsis* SWEET genes (AtSWEET4, AtSWEET5, AtSWEET7, AtSWEET13) also function in glucose transport when expressed in yeast or HEK293T cells (Supplementary Figs 5, 11 and 12).

Potential role of SWEETs in pathogen nutrition

Many pathogens acquire glucose from their hosts[9,11,13], thus pathogens may highjack host sugar efflux systems dedicated for plant development. We tested whether mRNA levels of

Arabidopsis SWEET family members were altered by challenge with bacterial and fungal pathogens. *Pseudomonas syringae* pv. *tomato* strain DC3000 infection highly induced mRNA levels of *AtSWEET4*, *AtSWEET5*, *AtSWEET7*, *AtSWEET8*, *AtSWEET10*, *AtSWEET12* and *AtSWEET15* in *Arabidopsis* leaves (Fig. 2). In contrast, the DC3000 type III secretion mutant (Δ*hrcU*), which cannot inject type III effector proteins into the host and is compromised in pathogenicity, did not induce three of the seven *AtSWEET* genes, demonstrating that *SWEET* mRNA abundance is modulated in a type-III-dependent manner (Fig. 2b). The fungal powdery mildew pathogen *Golovinomyces cichoracearum* induced a different set of *AtSWEET* mRNAs, most prominently *AtSWEET12* (Fig. 2a, c), and previous expression data have shown that infection with the fungal pathogen *Botrytis cinerea* induces expression of *AtSWEET4*, *AtSWEET15* and *AtSWEET17* (ref. [28]). Pathogen-specific modulation of SWEET mRNA levels, therefore, probably alters sugar efflux at the site of infection, having an impact on pathogen growth and plant immunity.

OsSWEET11 underlies the dominant allele (*Xa13*) of the recessive resistance gene *xa13* (refs [21, 29, 30]). Susceptibility alleles of *xa13* confer disease resistance against bacterial blight and have been isolated from geographically diverse rice accessions[30]. All alleles tested carry mutations in the promoter region of the *OsSWEET11* gene and interfere with pathogen-specific induction of the gene[21,31]. RNA interference of rice *OsSWEET11* confers resistance to the *Xanthomonas oryzae* pathovar *oryzae* (Xoo) strain PXO99^{A}, which otherwise grows in the apoplasm and xylem of the host. OsSWEET11 may, therefore, supply sugars to the pathogen by a uniport mechanism as demonstrated for the *Arabidopsis* homologues (Fig. 1a–h and Supplementary Figs 10–12). Consistent with cellular import/efflux functions, OsSWEET11 localizes to the plasma membrane in rice callus[29]. OsSWEET11 is less efficiently targeted to the plasma membrane of HEK293T cells compared to AtSWEET1 (Fig. 3a). Nevertheless, weak uptake activity was observed in HEK293T cells and oocytes (Fig. 3b, c).

Infection of rice by Xoo PXO99^{A} requires the bacterial type III effector gene *pthXo1* (ref. [21]). PthXo1 is a TAL (transcriptional activator-like) effector, which directly interacts with the *OsSWEET11* promoter as shown by chromatin immune precipitation (Fig. 3d), as well as transient co-expression in *Nicotiana benthamiana* leaves (Supplementary Fig. 13)[32,33]. PthXo1 secreted by Xoo PXO99^{A} specifically activates transcription of *OsSWEET11* (ref. [21]), presumably to induce sugar efflux to feed bacteria in the xylem and/or apoplasm (Fig. 4a). When *pthXo1* is mutated (as in strain PXO99^{A}ME2), transcription of *OsSWEET11* and pathogenicity are reduced[21], consistent with a model of sugar supply limiting growth of the pathogen (Fig. 4b). If OsSWEET11 becomes unavailable owing to mutations in the TAL effector binding element of the *OsSWEET11* promoter, or through RNA interference[21,31], the sugar supply becomes limiting and the pathogen cannot grow efficiently (Fig. 4c). Indeed, *ossweet11* (*xa13*) mutants are resistant to PXO99^{A} (ref. [21]). *xa13*-mediated resistance can be defeated by PXO99^{A} expressing the alternative TAL effector gene *avrXa7* (Fig. 4d), compatible with the most parsimonious hypothesis that another OsSWEET gene is co-opted by the pathogen to support bacterial growth[21]. Indeed, AvrXa7 activates the paralogue OsSWEET14 (ref. [33]). OsSWEET14 is targeted more efficiently to the plasma membrane in HEK293T cells (Fig. 3e) and mediates glucose import in HEK293T cells and oocytes (Fig. 3c, f, h and Supplementary Fig. 14). OsSWEET14 also functions as a low-affinity transporter(Fig. 3h), mediating efflux in both HEK293T cells and oocytes (Fig. 3g, i). Our findings support a model that, besides inhibition of plant immunity, type III effectors and some TAL effectors can function specifically in diverting nutritional resources from the host[34,35].

Metazoan SWEETs as glucose transporters

SWEET homologues (SLC50) are also widespread in metazoan genomes and predicted to consist of seven transmembrane helices in a 3+1+3 configuration (Fig. 1j and Supplementary Figs 8 and 9). The *C. elegans* genome contains seven *SWEET* genes (*CeSWEET*), whereas the human genome contains a single homologue, which we name *HsSWEET1* (also called *RAG1AP1*). CeSWEET1 mediated glucose accumulation in HEK293T cells when co-expressed with the sensor FLII^{12}Pglu700μδ6 (ref. [16]), as well as efflux from the cytosol to the ER (Fig. 5a, b). Both N- and C-terminal GFP fusions of CeSWEET1 were functional in cellular glucose uptake (Supplementary Fig. 15) and localized primarily to the Golgi, with lower levels at the plasma membrane of HEK293T cells (Fig. 5c, d). CeSWEET1 mediated [^{14}C]glucose and [^{14}C]galactose uptake when expressed in oocytes (Fig. 5e, f). Similar to OsSWEET14, CeSWEET1 glucose uptake did not saturate up to 50 mM, indicating that it is a low-affinity transporter (Fig. 5g). CeSWEET1 expression in oocytes can also increase glucose efflux (Fig. 5h). RNAi inhibition of CeSWEET1 affected fat accumulation in worms, compatible with a defect in cellular glucose efflux leading to lipid accumulation[36]. Mutations in the homologue CiSWEET1/Ci-RGA from the sea squirt *Ciona* leads to early developmental defects, underlining the importance of SWEETs in metazoa[37].

The human homologue HsSWEET1 did not show significant glucose uptake in yeast and oocytes (Fig. 5e and Supplementary Figs 6 and 11). However, HsSWEET1 mediated weak efflux activity in oocytes (Fig. 5i). The efflux activity was not caused by unspecific leakiness of oocytes as efflux of other sugars was not increased in cells expressing HsSWEET1 or CeSWEET1 (Supplementary Fig. 16). Thus, HsSWEET1 either rectifies or, alternatively, might be involved in exocytosis. In contrast to the plant homologues, and compatible with vesicular efflux, HsSWEET1 localized to the Golgi of HEK293T cells with minimal presence at the plasma membrane (Fig. 5j and Supplementary Figs 17–19). Mutation of the potential di-leucine internalization motif at the C terminus[38] did not lead to increased plasma membrane localization or increased transporter activity (Fig. 5e and Supplementary Fig. 18). Expression data indicate ubiquitous expression throughout human tissues and cell lines, with highest expression in oviduct, epididymis and intestine (Supplementary Fig. 20). Immunolocalization data from the Human Protein Atlas are consistent with a localization in absorptive enterocytes[39,40]. Moreover, mouse *MmSWEET1* expression was induced in the mammary gland during lactation (Supplementary Fig. 21). Localization is compatible with a function in supplying glucose to the Golgi for lactose synthesis and secretion[41].

Our findings provide new insights into processes that involve sugar efflux from human cells. The human genome contains two additional classes of glucose transporters[42]. GLUTs are uniporters, whereas SGLTs are Na^+-coupled co-transporters. GLUTs and SGLTs probably handle most of the uptake activities found in human cells. GLUT2 had originally been thought to be responsible for both import and efflux of glucose in liver and intestine. However, glucose efflux from GLUT2-null hepatocytes and GLUT2 knockout mice appeared unaffected[2–4]. Oral glucose load of GLUT2 knockout mice resulted in normal rates of glucose appearance in the blood[2]. Similarly, people affected with Fanconi–Bickel syndrome, caused by GLUT2 mutations[43], do not show abnormal carbohydrate ingestion, a process that requires efflux from intestinal cells[44]. These findings led to the hypothesis for alternative efflux routes[3,4]. HsSWEET1 is thus a candidate for the postulated alternative vesicular glucose efflux from the intestine and liver cells (Supplementary Fig. 22).

A new class of sugar transporters is described, members of which have been shown to function as uniporters and are thus able to support import and efflux of sugars from cells.

SWEETs undoubtedly have many important native functions, including the supply of carbon skeletons and energy to the gametophyte in plants and cellular glucose efflux in animals. Our findings also support the model that in addition to the inhibition of plant immunity, type III effectors are involved in accessing nutritional resources of host plants[34,35]. Notably, the founding member of the SWEET family, MtN3, was identified as a nodulin-specific EST in the legume *Medicago truncatula* and may have a role in symbiotic *Rhizobia*[45] nutrition. Knowledge of the full spectrum of pathogen effector molecules, and how they manipulate plant transport and metabolism to favour pathogen growth, will improve our understanding of host–pathogen interactions and may lead to new strategies for combating pathogen infections, which at the global scale lead to crop losses of over 10% annually[46]. Moreover, analysis of the complete SWEET family may help to solve some of the mysteries of pollen nutrition, nectar production and carbon sequestration.

METHODS SUMMARY

Cell culture, transfection, image acquisition and FRET analysis were performed as described previously[15]. Yeast complementation and uptake assays were performed in EBY4000 (ref. [17]). Tracer uptake and efflux assays were performed in *Xenopus* oocytes[47]. *Arabidopsis* Col-0 plants were grown in growth chambers under 8 h light/16 h dark at 22 °C. qPCR was performed with gene-specific primers (Supplementary Table 1). See Methods for details.

METHODS

qPCR and RT–PCR analysis

Total RNA was extracted from HepG2 or HEK293T cells using an RNeasy MINI kit (Qiagen), first strand cDNA was produced (New England Biolabs) and fragments of the predicted length were obtained by RT–PCR using a set of GLUT and SGLT primers published previously[48]. Samples were separated on a 2% agarose gel. For samples inoculated by *Pseudomonas syringae* pv. *tomato* DC3000, total RNA was extracted from the leaves using Trizol reagent (Invitrogen). Real-time quantitative PCR (qPCR) was performed using HotStart-IT SYBR Green qPCR Master Mix (USB) according to the manufacturer's instructions on a 7300 PCR system (Applied Biosystems). Actin (*ACT8*) expression was used to normalize expression values in each sample; expression values were determined relative to the value of the sample infiltrated with 1 mM $MgCl_2$ buffer at each time point using the comparative $2^{-\Delta\Delta Ct}$ method[49]. For samples infected by *G. cichoracearum* or *X. oryzae* pv. *oryzae*, qPCR assays were performed using a LightCycler 480 (Roche). For quantification, relative transcript levels for each gene were normalized to *ACT8* following the $2^{-\Delta\Delta Ct}$ method[49]. Fold change was calculated relative to the untreated sample. Analysis was repeated twice independently. The observed induction is confirmed by microarray data (Genevestigator)[50].

Constructs

AtSWEET1, *AtSWEET8*, *OsSWEET11* and *OsSWEET14* ORFs were amplified by RT–PCR using specific primers from *Arabidopsis* and rice, respectively. First-strand cDNA from rice was provided by P. Ronald. SWEET ORFs were cloned into pDONR221 (Invitrogen) or pDONR221-f1 (ref. [51]). Truncated versions of AtSWEET1-L198*, OsSWEET11-F205* and OsSWEET14-F203* were generated by introducing stop codons in transmembrane helix 7 by site-directed mutagenesis. All entry constructs were transferred to pDRf1-GW (ref. [52]) and pOO2-GW (D. Loqué, unpublished results) by Gateway LR recombination reactions (a recombination reaction between an entry clone (containing attL) and a destination vector (containing attR), mediated by a host of recombination proteins to generate an expression clone (Entry Clone + Destination Vector Expression Clone)) (Invitrogen). *AtSWEET1* was

cloned into p112-A1NE-GW for yeast co-transformation with FLII^{12}Pglu700μδ6 in pDRf1-GW (ref. [18]). Plasmid p112-A1NE-GW was generated by inserting a Gateway cassette into the SmaI restriction site of p112-A1NE[53]. For radiotracer experiments, ORFs with stop codons for *AtSWEET1*, *OsSWEET11* and *OsSWEET14* were cloned into the pOO2-GW by Gateway LR recombination reactions.

The full-length splice variant *HsSWEET1-1* in pDNR-LIB was obtained from Open Biosystems (Clone ID 4076256). The truncated form HsSWEET1-G194* was generated by introducing a stop codon at leucine 194 by site-directed muta-genesis[54]. Site-directed mutagenesis was used to mutate the putative internalization motif (HsSWEET1m Y216A, L218A, L219A). Products were cloned by *in vitro* BP recombination (Invitrogen) into pDONR221-f1, then mobilized into pOO2-GW by LR reactions. The shorter splice variant *HsSWEET1-2* from Open Biosystems (Clone ID 3896154) in pCMV-SPORT6 was transferred into pOO2-GW by *in vitro* LR recombination. *CeSWEET1* (K02D7.5, Open Biosystems) was cloned into pOO2-GW using an LR reaction. The ORF of *AtSWEET1* without stop codon was cloned into the binary vector pX-YFP-GW by an LR reaction. *AtSWEET1*, *OsSWEET11*, *OsSWEET14*, *CeSWEET1* and *HsSWEET1* without stop codons were cloned into C-terminal GFP fusion vector pcDNA-DEST47 (Invitrogen) for localization studies. *AtSWEET1*, *CeSWEET1* and *HsSWEET1*with stop codons were cloned into the N-terminal GFP fusion vector pcDNA-DEST53 (Invitrogen) for localization studies. For yeast growth assays, ORFs were expressed from pDRf1-GW. For GFP localization in yeast, *AtSWEET1* and the truncated AtSWEETΔ198 were cloned in vector pDR-GW-eGFP[52].

FRET analysis

Mammalian cell culture, transfection, image acquisition and FRET analysis were performed as described[15,55].

Yeast expression

The strain EBY4000 (*hxt1* through *-17*Δ::*loxP gal2*Δ::*loxP stl1*Δ::*loxP agt1*Δ::*loxP ydl247w*Δ::*loxP yjr160c*Δ::*loxP*)[17] was transformed with *AtSWEET1*, *AtSWEET8* and HXT5 and grown on SD (synthetic deficient) medium supplemented with 2% maltose and auxotrophic requirements. For complementation growth assays, cells were grown overnight in liquid minimum medium to an optical density at 600 nm (OD_{600}) of ~0.6, then OD_{600} was adjusted to ~0.2 with water. Serial dilutions (×1, ×5, ×25 and ×125) were plated on SD media containing either 2% maltose (as control) or 2% glucose plus respective auxotrophic requirements. Growth was documented by scanning (CanoScan, Canon) after 2–5 days at 30 °C.

Yeast uptake

Yeast cells were grown in SD medium supplemented with 2% maltose and auxotrophic markers. Cells were harvested at OD_{600} 0.5–0.7 by centrifugation, and washed twice in ice-cold distilled water. Cell pellets were weighed after supernatant had been removed. Cells were re-suspended 5–10% (w/v) in 40 mM potassium phosphate buffer, pH 6.0. Cells were pre-incubated in potassium phosphate buffer for 5 min at 30 °C. For each reaction, 330 μl pre-warmed buffer containing 20 mM glucose (0.55 μCi D-[U-^{14}C] glucose; 590 kBq μmol^{-1}, Amersham) was added to an equal volume of cells. 120 μl aliquot were withdrawn and transferred to ice-cold water. Cells were harvested by vacuum filtration onto a glassfibre filters (GF/C, Whatman), and washed twice in 10 ml ice-cold water. Filters were transferred to scintillation vials containing 5 ml Ultima Gold XR Scintillation liquid (Perkin Elmer). Radioactivity taken up by the cells was measured by liquid scintillation spectrometry. To determine the pH-dependence of AtSWEET1 activity, 40 mM potassium phosphate uptake

buffer at specified pH was used. Three independent transformants were used for each uptake experiment.

Xenopus oocytes isolation and RNA injection

After linearization of the pOO2 plasmids with MluI, capped cRNAs were synthesized *in vitro* by SP6 RNA poly-merase using mMESSAGE mMACHINE kit (Ambion, Inc.). *Xenopus laevis* oocytes were provided by M. Goodman. Microinjection was carried out as described[47,56]. 25–50 ng cRNA was injected into healthy looking oocytes (RNase-free water was used as control). Oocytes expressing AtSWEET1 were maintained at 18 °C in modified Barth's saline (MBS, in mM: 88 NaCl, 1 KCl, 2.4 $NaHCO_3$, 0.82 $MgSO_4$, 0.33 $Ca(NO_3)_2$, 0.41 $CaC1_2$, 20 HEPES-Tris, pH 7.5) with 100 μM gentamycin, 100 U ml^{-1} penicillin and 100 μM streptomycin solution for 2–3 d. Incubation buffer was changed every 24 h. For all other SWEETs, injected oocytes were maintained in L-15 oocyte medium (7.4 g l^{-1} Leibovitz's L-15 medium (Sigma), 3.57 g l^{-1} HEPES pH 7.5) with 100 mg l^{-1} gentamycin.

Tracer uptake in *Xenopus* oocytes

The assay was performed with modification as described previously[57]. Two days after injection, groups of 7–16 oocytes were transferred into tubes containing 200 μl Na-Ringer (in mM: 115 NaCl, 2 KCl, 1 $MgCl_2$, 1.8 $CaC1_2$, 10 HEPES-Tris, pH 7.5) 100 mg l^{-1} gentamycin and D-glucose (4 μCi ml^{-1} D-[^{14}C(U)]-glucose; PerkinElmer), galactose (4 μCi ml^{-1} D[1-^{14}C]-galactose; American Radiolabelled Chemicals) or sucrose (4 μCi ml^{-1} D-[1-^{14}C(U)]-sucrose; PerkinElmer). After incubation at 20 °C, cells were transferred to ice-cold Na-Ringer, washed three times, solubilized with 100 μl 1% (w/v) SDS, and measured individually.

Tracer efflux assay in *Xenopus* oocytes

Efflux was measured as described[58]. Two days after cRNA injection, oocytes were injected with 50 nl solution containing 5, 10 or 50 mM -glucose or sucrose with 0.18 μCi μl^{-1} D-[^{14}C(U)]glucose. Cells were immediately washed once in Na-Ringer (except AtSWEET1 in MBS). At defined time points, reaction buffer (450 μl; except AtSWEET1 in 950 μl) was removed for scintillation counting. Oocytes were solubilized with 1% SDS and analysed for retained radioactivity.

Analysis of glucose accumulation in yeast cells by FRET sensors

FRET measurements in yeast cells were performed as described[18].

Plant growth and pathogen infection

Arabidopsis Col-0 plants were grown in growth chambers under 8 h light/14 h dark at 22 °C. Five-week-old leaves were infiltrated with a 1 mM $MgCl_2$ buffer, 2×10^8 c.f.u. ml^{-1} *Pseudomonas syringae* pv. *tomato* DC3000 or *Pseudomonas syringae* pv. *tomato* DC3000 *Δ hrcU* suspensions in 1 mM $MgCl_2$ using needleless syringes. Leaf samples were collected after 6, 12 and 24-h incubation in the light. *G. cichoracearum* inoculation was performed as described[59]. Plants were placed in a 'settling tower' (cardboard box) and inoculated with *G. cichoracearum* spores by holding infected squash leaves over the settling tower and using compressed air (duster cans) to blow spores off of the squash leaves for settling onto *Arabidopsis* plants. Inoculum density was ~25–35 conidiospores per mm^2. After inoculation, plants were incubated for 1 h in a dark dew chamber, then transferred to a growth chamber at 16 h day length, 70% relative humidity.

Chromosome immune precipitation (ChIP) assay

Two-week-old rice seedlings (cultivar IR24) were infected with Flag-tagged effector *X. oryzae* pv. *oryzae* strains ME2(*avrXa7*-2F) or ME2(*pthXo1*-2F) at OD_{600} 0.5. At 20 h after inoculation, ChIP complexes were prepared from 3.0 g of inoculated leaf tissue for each treatment. Immune complexes were prepared as described[60] with minor modifications. Effector-associated DNA complexes were immunoprecipitated using monoclonal Flag antibody (Sigma, 12 μg ml^{-1}). The same amount of mouse nonspecific IgG antibody was added in the control. Enriched DNA obtained was analysed by real-time qPCR using promoter and 3′ UTR specific primers (provided Supplementary Table 3). Two microlitres of eluted DNA was used in each reaction. qPCR and analysis was performed as described above. Values are expressed as a ratio of the $2^{-\Delta\Delta Ct}$ value from Flag-tagged antibody precipitate complexes over the $2^{-\Delta\Delta Ct}$ value of the nonspecific IgG complexes. $PXO99^{A}ME2$ (*avrXa7-F2*) served as control for effector specificity.

Alignment and phylogenetic analysis

Multiple alignment of SWEET amino acid sequences was performed with CLUSTALW[61] using default parameters, and a phylogenetic analysis was performed using the software Mega V3.1. Bootstrapping was performed 1,000 times to obtain support values for each branch. For pair-wise comparison, multiple alignments of complete amino acid sequences were conducted using the Vector NTI advance 11.0.

Confocal microscopy

Fluorescence imaging of plants and mammalian cells expressing AtSWEET1–YFP, AtSWEET8–YFP, CeSWEET1–GFP, GFP–CeSWEET1, OsSWEET11–GFP and OsSWEET14–GFP was performed on a Leica TCS SP5 microscope. YFP was visualized by excitation with an argon laser at 514 nm and spectral detector set between 525 and 560 nm for the emission. GFP was visualized by excitation with an argon laser at 488 nm and spectral detector set between 500 and 545 nm for the emission. Specimens were observed with 40/0.75-1.25NA HCX PL APO CS objective.

Supplementary Material

Refer to Web version on PubMed Central for supplementary material.

Acknowledgments

This work was made possible by grants from the Department of Energy (DE-FG02-04ER15542) and NIH (NIDDK; 1RO1DK079109) to W.B.F., X.-Q.Q. was supported by The Carnegie Institution and the National Natural Science Foundation of China (NSFC; 30771288). NSF (IOS-0821801) and NIH (ZRO1GM06886-06A1) to M.B.M. and J.-G.K. was supported 50% by NIH and 50% by NSF. W.U. was supported in part by an NIH postdoctoral fellowship (F32GM083439-02). G.A. and F.F.W. were supported by grants from USDA NIFA (2007-35319-18103) and NSF Plant Genome (DBI-0820831).

References

1. Lalonde S, Wipf D, Frommer WB. Transport mechanisms for organic forms of carbon and nitrogen between source and sink. Annu Rev Plant Biol. 2004; 55:341–372. [PubMed: 15377224]
2. Thorens B, Guillam MT, Beermann F, Burcelin R, Jaquet M. Transgenic reexpression of GLUT1 or GLUT2 in pancreatic β cells rescues GLUT2-null mice from early death and restores normal glucose-stimulated insulin secretion. J Biol Chem. 2000; 275:23751–23758. [PubMed: 10823833]
3. Stümpel F, Burcelin R, Jungermann K, Thorens B. Normalkinetics of intestinal glucose absorption in the absence of GLUT2: evidence for a transport pathway requiring glucose phosphorylation and transfer into the endoplasmic reticulum. Proc Natl Acad Sci USA. 2001; 98:11330–11335. [PubMed: 11562503]

4. Hosokawa M, Thorens B. Glucose release from GLUT2-null hepatocytes: characterization of a major and a minor pathway. Am J Physiol Enocriol Metab. 2002:E794–E801.
5. Hesse, M.; Pacini, E.; Willemse, M. The Tapetum: Cytology, Function, Biochemistry and Evolution. Springer; 2004. p. 1-152.
6. Bisseling T, Dangl JL, Schulze-Lefert P. Next-generation communication. Science. 2009; 324:691. [PubMed: 19423780]
7. Zhou Y, Qu H, Dibley KE, Offler CE, Patrick JW. A suite of sucrose transporters expressed in coats of developing legume seeds includes novel pH-independent facilitators. Plant J. 2007; 49:750–764. [PubMed: 17253986]
8. Tang DJ, et al. *Xanthomonas campestris* pv. *campestris* possesses a single gluconeogenic pathway that is required for virulence. J Bacteriol. 2005; 187:6231–6237. [PubMed: 16109965]
9. Patrick JW. Solute efflux from the host at plant microorganism interfaces. Aust J Plant Physiol. 1989; 16:53–67.
10. Aked J, Hall JL. The uptake of glucose, fructose and sucrose into the lower epidermis of leaf discs of pea (*Pisum sativum* L. cv Argenteum). New Phytol. 1993; 123:271–276.
11. Sutton PN, Henry MJ, Hall JL. Glucose, and not sucrose, is transported from wheat to wheat powdery mildew. Planta. 1999; 208:426–430.
12. Sutton PN, Gilbert MJ, Williams LE, Hall JL. Powdery mildew infection of wheat leaves changes host solute transport and invertase activity. Physiol Plant. 2007; 129:787–795.
13. Voegele RT, Struck C, Hahn M, Mendgen K. The role of haustoria in sugar supply during infection of broad bean by the rust fungus *Uromyces fabae*. Proc Natl Acad Sci USA. 2001; 98:8133–8138. [PubMed: 11390980]
14. Aramemnon. Plant membrane protein database ⟨. 2010. http://aramemnon.botanik.uni-koeln.de⟩
15. Takanaga H, Frommer WB. Facilitative plasma membrane transporters function during ER transit. FASEB J. 2010; 24:2849–2858. [PubMed: 20354141]
16. Takanaga H, Chaudhuri B, Frommer WB. GLUT1 and GLUT9 as major contributors to glucose influx in HepG2 cells identified by a high sensitivity intramolecular FRET glucose sensor. Biochim Biophys Acta. 2008; 1778:1091–1099. [PubMed: 18177733]
17. Wieczorke R, et al. Concurrent knock-out of at least 20 transporter genes is required to block uptake of hexoses in *Saccharomyces cerevisiae*. FEBS Lett. 1999; 464:123–128. [PubMed: 10618490]
18. Bermejo C, Haerizadeh F, Takanaga H, Chermak D, Frommer WB. Dynamic analysis of cytosolic glucose and ATP levels in yeast with optical sensors. Biochem J. September 20.2010 10.1042/BJ20100946
19. Chaudhuri B, et al. Protonophore- and pH-insensitive glucose and sucrose accumulation detected by FRET nanosensors in *Arabidopsis* root tips. Plant J. 2008; 56:948–962. [PubMed: 18702670]
20. Guan YF, et al. RUPTURED POLLEN GRAIN1, a member of the MtN3/saliva gene family, is crucial for exine pattern formation and cell integrity of microspores in *Arabidopsis*. Plant Physiol. 2008; 147:852–863. [PubMed: 18434608]
21. Yang B, Sugio A, White FF. *Os8N3* is a host disease-susceptibility gene for bacterial blight of rice. Proc Natl Acad Sci USA. 2006; 103:10503–10508. [PubMed: 16798873]
22. Song LF, Zou JJ, Zhang WZ, Wu WH, Wang Y. Ion transporters involved in pollen germination and pollen tube tip-growth. Plant Signal Behav. 2009; 4:1193–1195. [PubMed: 20514245]
23. Engel ML, Holmes-Davis R, McCormick S. Green sperm. Identification of male gamete promoters in *Arabidopsis*. Plant Physiol. 2005; 138:2124–2133. [PubMed: 16055690]
24. Ge YX, et al. Partial silencing of the *NEC1* gene results in early opening of anthers in *Petunia hybrida*. Mol Genet Genomics. 2001; 265:414–423. [PubMed: 11405624]
25. Ge YX, et al. *NEC1*, a novel gene, highly expressed in nectary tissue of *Petunia hybrida*. Plant J. 2000; 24:725–734. [PubMed: 11135107]
26. Quirino BF, Reiter WD, Amasino RD. One of two tandem *Arabidopsis* genes homologous to monosaccharide transporters is senescence-associated. Plant Mol Biol. 2001; 46:447–457. [PubMed: 11485201]

27. Quirino BF, Normanly J, Amasino RM. Diverse range of gene activity during *Arabidopsis thaliana* leaf senescence includes pathogen-independent induction of defense-related genes. Plant Mol Biol. 1999; 40:267–278. [PubMed: 10412905]
28. Ferrari S, et al. Resistance to *Botrytis cinerea* induced in *Arabidopsis* by elicitors is independent of salicylic acid, ethylene, or jasmonate signaling but requires PHYTOALEXIN DEFICIENT3. Plant Physiol. 2007; 144:367–379. [PubMed: 17384165]
29. Yuan M, Chu Z, Li X, Xu C, Wang S. Pathogen-induced expressional loss of function is the key factor in race-specific bacterial resistance conferred by a recessive R gene *xa13* in rice. Plant Cell Physiol. 2009; 50:947–955. [PubMed: 19318375]
30. Chu Z, et al. Promoter mutations of an essential gene for pollen development result in disease resistance in rice. Genes Dev. 2006; 20:1250–1255. [PubMed: 16648463]
31. Chu Z, et al. Targeting *xa13*, a recessive gene for bacterial blight resistance in rice. Theor Appl Genet. 2006; 112:455–461. [PubMed: 16328230]
32. Boch J, et al. Breaking the code of DNA binding specificity of TAL-type III effectors. Science. 2009; 326:1509–1512. [PubMed: 19933107]
33. Antony G, et al. xa13 recessive resistance to bacterial blight is defeated by the induction of disease susceptibility gene *Os11N3*. Plant Cell. in the press.
34. Grant SR, Fisher EJ, Chang JH, Mole BM, Dangl JL. Subterfuge and manipulation: type III effector proteins of phytopathogenic bacteria. Annu Rev Microbiol. 2006; 60:425–449. [PubMed: 16753033]
35. Mansfield JW. From bacterial avirulence genes to effector functions via the hrp delivery system: an overview of 25 years of progress in our understanding of plant innate immunity. Mol Plant Pathol. 2009; 10:721–734. [PubMed: 19849780]
36. Ashrafi K, et al. Genome-wide RNAi analysis of *Caenorhabditis elegans* fat regulatory genes. Nature. 2003; 421:268–272. [PubMed: 12529643]
37. Hamada M, Wada S, Kobayashi K, Satoh N. *Ci-Rga*, a gene encoding an MtN3/saliva family transmembrane protein, is essential for tissue differentiation during embryogenesis of the ascidian *Ciona intestinalis*. Differentiation. 2005; 73:364–376. [PubMed: 16219040]
38. Ibberson M, Uldry M, Thorens B. GLUTX1, a novel mammalian glucose transporter expressed in the central nervous system and insulin-sensitive tissues. J Biol Chem. 2000; 275:4607–4612. [PubMed: 10671487]
39. Berglund L, et al. A genecentric Human Protein Atlas for expression profiles based on antibodies. Mol Cell Proteomics. 2008; 7:2019–2027. [PubMed: 18669619]
40. Human Protein Atlas. Small intestine [RAG1AP1] ⟨. 2010. http://www.proteinatlas.org/normal_unit.php?antibody_id=18095&mainannotation_id=1747049⟩
41. Anderson SM, Rudolph MC, McManaman JL, Neville MC. Key stages in mammary gland development. Secretory activation in the mammary gland: it's not just about milk protein synthesis! Breast Cancer Res. 2007; 9:204. [PubMed: 17338830]
42. Bioparadigms. SLC Tables. 2010. ⟨http://www.bioparadigms.org/slc/intro.htm⟩
43. Santer R, et al. Mutations in *GLUT2*, the gene for the liver-type glucose transporter, in patients with Fanconi-Bickel syndrome. Nature Genet. 1997; 17:324–326. [PubMed: 9354798]
44. Manz F, et al. Fanconi-Bickel syndrome. Pediatr Nephrol. 1987; 1:509–518. [PubMed: 3153325]
45. Udvardi MK, Yang LJO, Young S, Day DA. Sugar and amino acid transport across symbiotic membranes from soybean nodules. Mol Plant Micr Int. 1990; 3:334–340.
46. Oerke EC. Crop losses to pests. J Agric Sci. 2006; 144:31–43.
47. Hediger MA, Coady MJ, Ikeda TS, Wright EM. Expression cloning and cDNA sequencing of the Na^+/glucose co-transporter. Nature. 1987; 330:379–381. [PubMed: 2446136]
48. Fehr M, Takanaga H, Ehrhardt DW, Frommer WB. Evidence for high-capacity bidirectional glucose transport across the endoplasmic reticulum membrane by genetically encoded fluorescence resonance energy transfer nanosensors. Mol Cell Biol. 2005; 25:11102–11112. [PubMed: 16314530]
49. Livak KJ, Schmittgen TD. Analysis of relative gene expression data using real-time quantitative PCR and the $2^{-\Delta\Delta CT}$ method. Methods. 2001; 25:402–408. [PubMed: 11846609]

50. Hruz T, et al. Genevestigator v3: a reference expression database for the meta-analysis of transcriptomes. Adv Bioinformatics. 2008; 2008:420747. [PubMed: 19956698]
51. Lalonde S, et al. A membrane protein/signaling protein interaction network for Arabidopsis version AMPv2. Front Physiol. September 22.2010 10.3389/fphys.2010.00024
52. Loqué D, Lalonde S, Looger LL, von Wiren N, Frommer WB. A cytosolic trans-activation domain essential for ammonium uptake. Nature. 2007; 446:195–198. [PubMed: 17293878]
53. Riesmeier JW, Willmitzer L, Frommer WB. Isolation and characterization of a sucrose carrier cDNA from spinach by functional expression in yeast. EMBO J. 1992; 11:4705–4713. [PubMed: 1464305]
54. Kunkel TA, Bebenek K, McClary J. Efficient site-directed mutagenesis using uracil-containing DNA. Methods Enzymol. 1991; 204:125–139. [PubMed: 1943776]
55. Hou BH, Takanaga H, Griesbeck O, Frommer WB. Osmotic induction of calcium accumulation in human embryonic kidney cells detected with a high sensitivity FRET calcium sensor. Cell Calcium. 2009; 46:130–135. [PubMed: 19628278]
56. Ballatori N, Wang W, Li L, Truong AT. An endogenous ATP-sensitive glutathione S-conjugate efflux mechanism in *Xenopus laevis* oocytes. Am J Physiol. 1996; 270:R1156–R1162. [PubMed: 8928920]
57. Detaille D, Wiernsperger N, Devos P. Metformin interaction with insulin-regulated glucose uptake, using the *Xenopus laevis* oocyte model expressing the mammalian transporter GLUT4. Eur J Pharmacol. 1999; 377:127–136. [PubMed: 10448935]
58. Chernova MN, et al. Electrogenic sulfate/chloride exchange in *Xenopus* oocytes mediated by murine AE1 E699Q. J Gen Physiol. 1997; 109:345–360. [PubMed: 9089441]
59. Vogel J, Somerville S. Isolation and characterization of powdery mildew-resistant Arabidopsis mutants. Proc Natl Acad Sci USA. 2000; 97:1897–1902. [PubMed: 10677553]
60. Haring M, et al. Chromatin immunoprecipitation: optimization, quantitative analysis and data normalization. Plant Methods. 2007; 3:11. [PubMed: 17892552]
61. Thompson JD, Higgins DG, Gibson TJ. CLUSTAL W: improving the sensitivity of progressive multiple sequence alignment through sequence weighting, position-specific gap penalties and weight matrix choice. Nucleic Acids Res. 1994; 22:4673–4680. [PubMed: 7984417]

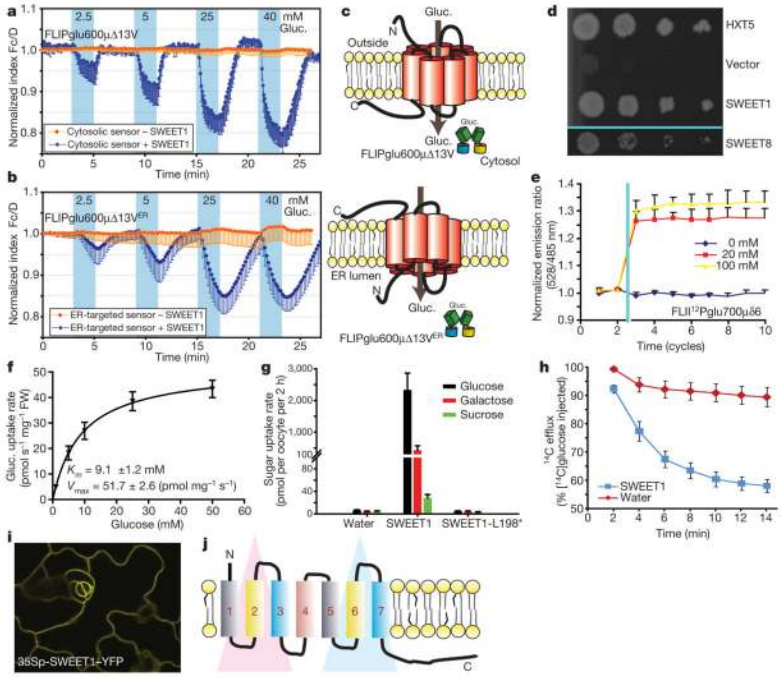

Figure 1. Characterization of SWEET transporters

a, Identification of glucose transport activity for AtSWEET1 by co-expression with cytosolic FRET glucose sensor FLIPglu600μΔ 13V in HEK293T cells[15]. Individual cells were analysed by quantitative ratio imaging of CFP and Venus emission (acquisition interval 5 s; Fc/D corresponds to normalized emission intensity ratio[15]). HEK293T/FLIPglu600μΔ 13V cells were perfused with medium, followed by square pulses of increasing glucose (Gluc.) concentrations. Orange line indicates cells expressing sensor alone; blue line indicates cells co-expressing sensor and AtSWEET1; accumulation of glucose is shown by a negative FRET ratio change (blue line; mean – s.d.; $n > 10$). **b**, FRET imaging of glucose efflux from cytosol into ER. FLIPglu600μΔ13V^{ER} was targeted to the ER lumen[15] (compare with panel **a**; acquisition interval 10 s; mean – s.d.; $n > 10$). **c**, Cartoon for SWEET influx across plasma membrane and efflux from cytosol to ER. Cytosolic FLIPglu600μΔ 13V identifies glucose import from the extracellular face (extracellular N terminus). FLIPglu600μΔ13V^{ER} measures transport from the intracellular side (cytosolic C terminus). **d**, Complementation of yeast EBY4000 (ref. [17]) lacking 18 hexose transporter genes with AtSWEET1, AtSWEET8, or yeast HXT5; control, empty vector. **e**, Glucose accumulation in EBY4000 co-expressing AtSWEET1 and FLII^{12}Pglu700μδ6 before and after glucose addition (two cycles before glucose addition; mean ± s.d.; $n = 3$). **f**, Kinetics of [^{14}C]glucose accumulation by AtSWEET1 in EBY4000 (mean ± s.d., $n = 3$). **g**, AtSWEET1-mediated uptake of 1 mM [^{14}C]glucose, [^{14}C]galactose or [^{14}C]sucrose into oocytes (mean ± s.d.; $n = 8$ cells). **h**, [^{14}C]glucose efflux from oocytes expressing AtSWEET1 (mean ± s.e.; $n \geq 10$ cells; $P < 0.0005$). **i**, Confocal imaging of AtSWEET1–YFP in leaves of stably transformed *Arabidopsis* (panel width = 176 μm). **j**, Structural model of SWEETs based on hydrophobicity plots (duplication of three transmembrane helices; red/blue triangles).

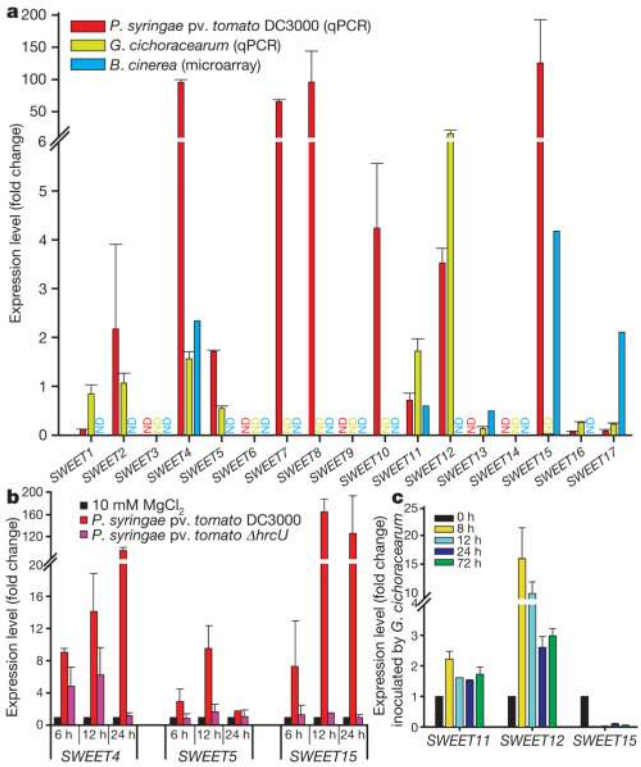

Figure 2. Biotrophic bacteria or fungi induce mRNA levels of different *SWEET* genes

a, Induction of *AtSWEET* mRNAs by either the bacterium *Pseudomonas syringae* pv. *tomato* DC3000 (2×10^8 c.f.u. ml^{-1}, 8 h after inoculation, measured by qPCR, normalized by $MgCl_2$ buffer treatment), powdery mildew fungus *G. cichoracearum* (~25–35 conidiospores per mm^2, 48 h after inoculation, measured by qPCR; normalized to 0 h values), or by *Botrytis cinerea* (from microarray study[28]) in *Arabidopsis* leaves. ND, not detectable. **b**, Induction of *AtSWEET4*, *AtSWEET5* and *AtSWEET15* by *P. syringae* DC3000 depends on a functional type III secretion system (T3S). Samples were collected at 6, 12 and 24 h after infiltration with 2×10^8 c.f.u. ml^{-1} of DC3000 or DC3000 *ΔhrcU*, a T3S mutant. **c**, Infection by *G. cichoracearum* leads to induction of *AtSWEET11* and *AtSWEET12* but downregulation of *AtSWEET15*.

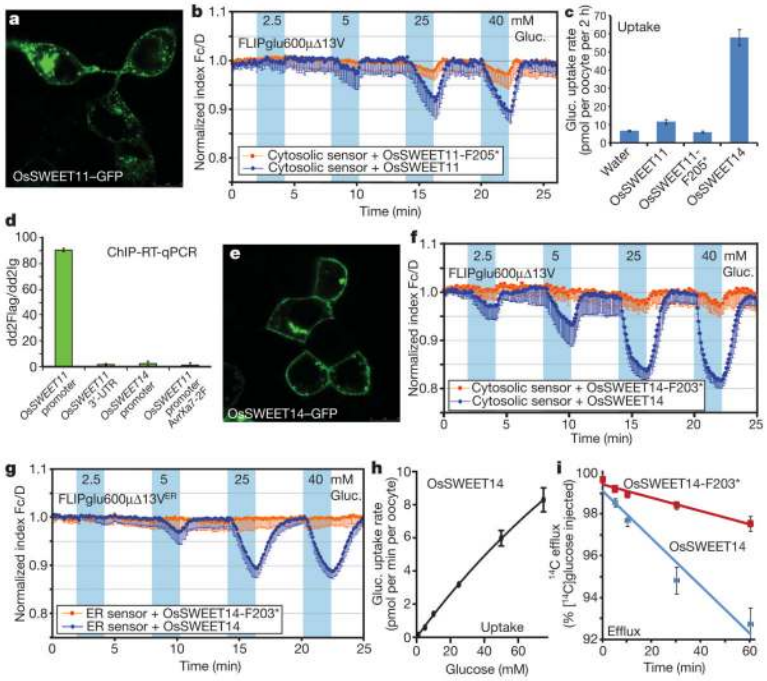

Figure 3. Type-III-effector-specific induction of *OsSWEET* genes in rice disease

a, Targeting of OsSWEET11 to the plasma membrane of HEK293T cells (panel width = 61 μm). **b**, Co-expression of OsSWEET11 with cytosolic FRET glucose sensor FLIPglu600μΔ13V in HEK293T cells (compare to Fig. 1a; significant above control in 4 of 6 experiments). Truncated OsSWEET11 with premature stop codon at phenylalanine 205 (F205*) served as negative control (mean – s.d., $n > 10$). **c**, Glucose uptake (1 mM) mediated by OsSWEET11 and OsSWEET14 in oocytes (mean ± s.d., $n \geq 7$). **d**, Enrichment of 5′-upstream *OsSWEET11* promoter DNA upon infection of rice with PXO99^{A} containing Flag-tagged PthXo1-2F. **e**, Efficient targeting of OsSWEET11 to the plasma membrane of HEK293T cells (panel width = 61 μm; mean ± s.d.; $n = 2$). **f**, Co-expression of OsSWEET14 with the cytosolic FRET glucose sensor FLIPglu600μΔ13V in HEK293T cells (compare to Fig. 1a). Truncated OsSWEET14 with a premature stop codon at phenylalanine 203 (F203*) served as negative control (mean – s.d., $n > 10$). **g**, Co-expression of OsSWEET14 with ER-targeted FRET glucose sensor FLIPglu600μΔ13V^{ER} in HEK293T cells (compare with Fig. 1b) (mean – s.d., $n > 10$). **h**, Concentration-dependent glucose uptake by OsSWEET14 in oocytes (mean ± s.d., $n \geq 7$). **i**, [^{14}C]-efflux from glucose-injected oocytes mediated by OsSWEET14 (50 nl of 50 mM glucose injected; mean ± s.e., $n \geq 7$).

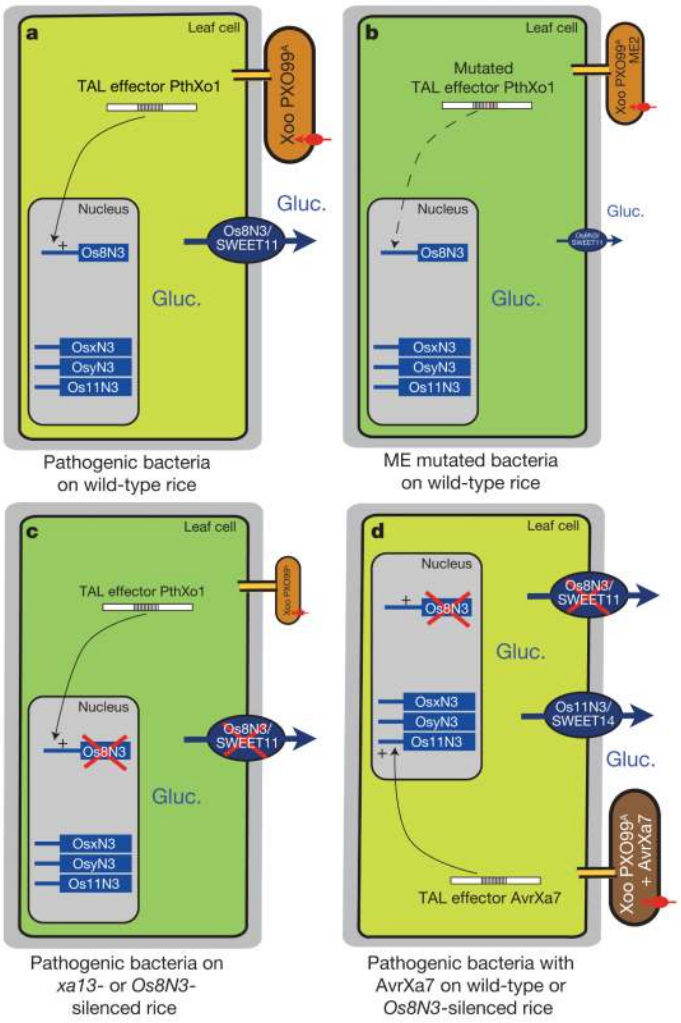

Figure 4. Model for the function of SWEET transporters in plant pathogenesis

a, The pathogenic Xoo strain PXO99^{A} injects TAL effector PthXo1 via the type III secretion system into rice cells. PthXo1 directly induces *OsSWEET11* leading to sugar efflux. Bacteria take up glucose and multiply. **b**, PXO99^{A} *pthXo1* mutant (PXO99^{A}ME2) leads to loss of *OsSWEET11* induction and reduced bacterial growth (indicated as reduced size of bacterium). **c**, Mutation of the *OsSWEET11* effector binding element (EBE) leads to loss of PthXo1-mediated induction and reduced bacterial growth. **d**, Bacteria expressing effector AvrXa7 can circumvent loss of *OsSWEET11* induction by inducing *OsSWEET14*.

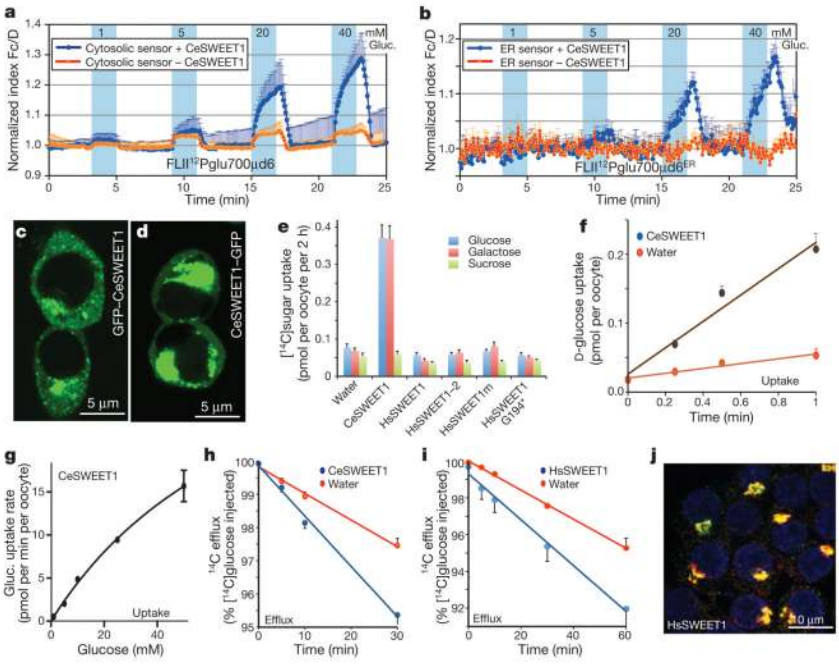

Figure 5. Metazoan SWEET transporters

a, Detection of CeSWEET1 glucose uptake in HEK293T cells by co-expressing FLII^{12}Pglu700μδ6 (see legend under Fig. 1a) (mean + s.d., $n \geq 10$). **b**, Detection of CeSWEET1 glucose efflux into the ER of HEK293T cells by co-expressing FLII^{12}Pglu700μδ6 (see legend under Fig. 1b) (mean + s.d., $n \geq 10$). **c**, **d**, Localization of GFP–CeSWEET1 (**c**) and CeSWEET1–GFP (**d**) fusions in HEK293T cells. **e**, [^{14}C]sugar uptake (5 mM) in *Xenopus* oocytes by CeSWEET1, HsSWEET1 (full length HsSWEET1; splice variant HsSWEET1–2; mean + s.d., $n \geq 8$), di-leucine motif mutant (HsSWEET1m) and deletion mutant G194*. **f**, Time-dependent [^{14}C]glucose uptake by CeSWEET1 in oocytes (mean + s.d., $n \geq 8$). **g**, Concentration-dependent [^{14}C]glucose uptake by CeSWEET1 in oocytes (mean ± s.d., $n \geq 8$). **h**, Efflux measurements from oocytes expressing CeSWEET1 (mean ± s.e.; $n \geq 8$ cells; $P < 0.01$ after 5 min; 50 nl of 50 mM sugar injected). **i**, Efflux measurements from oocytes expressing HsSWEET1 (mean ± s.e.; $n \geq 8$ cells; $P < 0.05$). **j**, Immunolocalization of HsSWEET1 in HEK293T cells (merged channels: immuno-labelled HsSWEET1, red; Golgi marker, green; nuclei, blue).